Title

- Cholesterol induces epithelial-to-mesenchymal transition of prostate cancer cells by suppressing degradation of EGFR through APMAP.

Running title: Cholesterol induces EMT via the APMAP-EPS15R-EGFR axis

Siyuan Jiang[1], Xuetong Wang[1], Dalong Song[2], XiaoJun Liu[1], Yinmin Gu[1], Zhiyuan Xu[1], Xiaodong Wang[1], Xiaolu Zhang[3], Qinong Ye[4], Zhou Tong[5], BingXue Yan[5], Jie Yu[7], Yunzhao Chen[7], Minxuan Sun[8], Yang Wang[5], and Shan Gao[1,5,6]*

Affiliations

1. CAS Key Laboratory of Bio-medical Diagnostics, Suzhou Institute of Biomedical Engineering and Technology, Chinese Academy of Sciences, Suzhou, 215163, China.
2. Department of Urology, GuiZhou provincial people's hospital, Guiyang, 550002, China.
3. Department of Medicine, The University of Toledo Health Sciences Campus, 3000 Arlington Ave, Toledo, OH 43614, The United States.
4. Department of Medical Molecular Biology, Beijing Institute of Biotechnology, Collaborative Innovation Center for Cancer Medicine, Beijing 100850, China.
5. Shanxi Academy of Advanced Research and Innovation, Taiyuan, 030032, China.
6. Medical College, Guizhou University, Guiyang, 550025, China.
7. Department of Pathology, the people's hospital of Suzhou National Hi-Tech District, Suzhou 215010, China
8. Jiangsu Key Lab of Medical Optics, Suzhou Institute of Biomedical Engineering and Technology, Chinese Academy of Sciences, Suzhou, China.

* Author for correspondence (gaos@sibet.ac.cn)

Competing interests: The authors declare that they have no competing interests.

Abstract

Cholesterol increases the risk of aggressive prostate cancer (PCa), and has emerged as a potential therapeutic target for PCa. The functional roles of cholesterol in PCa metastasis are not fully understood. Here we found that cholesterol induces the epithelial-to-mesenchymal transition (EMT) through extracellular regulated protein kinases 1/2 pathway activation, which is mediated by epidermal growth factor receptor (EGFR) and adipocyte plasma membrane-associated protein (APMAP) accumulation in cholesterol-induced lipid rafts. Mechanistically, APMAP increases the interaction with epidermal growth factor receptor substrate 15-related protein (EPS15R) to inhibit the endocytosis of EGFR by cholesterol, thus promoting cholesterol-induced EMT. Both the mRNA and protein levels of APMAP are upregulated in clinical PCa samples. Together, these findings shed light onto an APMAP/EPS15R/EGFR axis that mediates cholesterol-induced EMT of PCa cells.

Introduction

Although several treatments may benefit patients with localized prostate cancer (PCa), metastatic PCa remains lethal, and patients with metastatic PCa receive limited benefits from these treatments (1). Metastasis is a complex process, and this process involves the infiltration of cancer cells from the primary tumor site into the blood or lymphatic system, followed by extravasation into distant organs and the survival of invaded cells in suitable tissues to undergo metastatic colonization (2). Cancer cell metastasis requires a process known as the epithelial-to-mesenchymal transition (EMT), in which epithelial cells lose cell-cell adhesion properties and cell polarity and undergo reorganization of their cytoskeleton, dramatic changes in morphology and reprogramming of gene expression (3). This process is driven by activation of and/or crosstalk between several signaling pathways (4-6), including the transforming growth factor-β (TGF-β), epidermal growth factor/ EGF receptor (EGF/EGFR) and androgen receptor (AR) signaling pathways (7, 8). The key components of EMT are frequently deregulated in aggressive prostate cancer (7, 9).The underlying molecular mechanisms of EMT in prostate cancer remain poorly understood.

Cholesterol is a steroidal lipid that accumulates in cancer tissues and plays an essential role in the tumorigenesis of various cancers, such as colorectal, prostate, and breast cancers (10-12). Emerging evidence suggests that cholesterol is associated with the development of PCa and may serve as a diagnostic marker and therapeutic target for PCa (13-19). Furthermore, cholesterol-lowering drugs (statins) reduce the risk of advanced PCa (20, 21). Cholesterol elevation has been shown to promote tumor growth and reduce the apoptosis of PCa cells through the AKT signaling pathway and cyclin E (22, 23). However, the effect of cholesterol on EMT and the underlying mechanism are unclear in PCa.

Adipocyte plasma membrane-associated protein (APMAP) is characterized as a transmembrane protein and specifically induced during adipocyte differentiation and obesity (24-27). Epidermal growth factor receptor substrate 15-related protein (EPS15R) has been reported to regulate the internalization of EGFR (28). In this study, we demonstrate that APMAP participates in the cholesterol-induced EMT of PCa cells by reducing EGFR endocytosis. We show the cholesterol increase the interaction APMAP and EPS15R, thus influencing EGFR trafficking (28, 29). And we highlight APMAP as a potential diagnostic and therapeutic target for PCa.

Materials and Methods

Cell culture

All cell lines were obtained from the cell bank of type culture collection of Chinese academy of sciences and verified by short tandem repeat assays for their identification. Mycoplasma testing were performed by PCR every month. Cells were thawed from the original stocks and cultured do not exceed three weeks for experiments. 22Rv1 and DU-145 cells were cultured in DMEM (Gibco by Invitrogen, Carlsbad, Calif), and PC-3 cells were cultured in RPMI-1640 (Gibco by Invitrogen, Carlsbad, Calif); the media were supplemented with 10% fetal bovine serum (FBS, Gibco by Invitrogen, Carlsbad, Calif). Cells treated with cholesterol were cultured in medium containing 1% FBS. The cholesterol was mixed with 125uM fat free bovine serum albumin in medium containing 0.5% FBS before added to the cells.

Antibodies

Antibodies against N-cadherin, EPS15R, caveolin-1, flotillin-1, ATP1A1, GAPDH and vimentin were purchased from Abcam (Cambridge, MA, USA); rabbit anti-APMAP was purchased from Proteintech Group (Wuhan, Hubei, China); mouse monoclonal anti-APMAP was purchased from OriGene (Rockville, MD, USA); anti-mouse secondary antibody (HRP) for the Western blotting detection immunoprecipitation proteins was purchased from Abcam (Cambridge, MA, USA); preabsorbed Alexa Fluor 488- and 555-conjugated secondary antibodies were purchased from Abbkine (Wuhan, Hubei, China); preabsorbed Alexa Fluor 647-conjugated secondary antibodies were purchased from Jackson (West Grove, PA, USA); and the other 10 antibodies were purchased from Cell Signaling (Boston, MA,USA).

Immunoprecipitation and Western blot analysis

For co-immunoprecipitation (Co-IP), cells were lysed using Co-IP lysis buffer (20 mM Tris (pH 7.5), 150 mM NaCl, and 1% Triton X-100) supplemented with a protease and phosphatase inhibitor cocktail. The supernatants of the lysates were collected after centrifugation and then incubated with the indicated antibodies overnight at 4°C with constant rotation. Then, the antibodies in the lysates were precipitated with protein A/G magnetic beads (Millipore Billerica, MA, USA) and washed with PBS. Proteins were separated by SDS-PAGE, transferred to PVDF membranes (Millipore, Billerica, MA, USA), and detected with corresponding primary antibodies and HRP-conjugated secondary antibodies. Protein bands were visualized with the ChemiScope 6000 Touch Imaging system (Clinx, SHH, China).

Co-IP-MS/MS and data analysis

Co-IP was performed using FLAG M2 beads as described above. Proteins were eluted with 3×FLAG-peptide (Sigma) in PBS for 10 min. Proteins were precipitated with 20% trichloroacetic acid (TCA), and the resultant pellet was washed once with 10% TCA and 3 times with cold acetone. LC-MS/MS analysis was performed by Guangzhou Fitgene

Biotechnology Co. Briefly, the gel was cut into slices, the gel fragments were digested, and the residing peptides were extracted and lyophilized for further analysis. Peptides were suspended in 2% acetonitrile and 0.1% formic acid. For the LC run, samples were loaded onto a 75 μm i.d. ×150 mm reversed-phase column, packed with Acclaim PepMap RSLC C18. Separated peptides were directly analyzed with the mass spectrometer (Thermo Scientific Q Exactive) for online detection. The resulting spectra were recorded for each run. MS data were searched on Sorcerer2-SEQUEST using the reviewed Swiss-Prot database.

Expression vectors, shRNA and siRNA

APMAP was cloned with 3×FLAG or GFP at the 3'-terminus into the pLVX-puro lentivirus expression vector. EGFR was cloned with RFP/EGFP at the 3'-terminus into the expressionvector.Rab5-RFP and EPS15R-RFP vectors were obtained from Sino Biological (Beijing China). Short hairpin RNA (shRNA) for APMAP (target sequences: 5'-GGTGTTCTGCATCCAAATACG-3' and 5'-GGGACTATTTGAAGTAAATCC-3') were prepared by cloning double-stranded oligonucleotides into the vector pLVX. The siRNAs for EPS15R (target sequences: 5'-AAUUUAGGCGGUGGCAUGCTT-3' and 5'-UUUCUCUUUGUAACUGGTT-3') and MyD88-adapter-like (MAL) (target sequences: 5'-GCCCACGGUGGAGAGACUUTT-3' and 5'-CCGUGGUGUUCUCCUACAUTT-3') were from GenePharma (Shanghai, China).

Immunofluorescence

Cells were fixed with 4% paraformaldehyde for 15 min and permeabilized with 0.5% Triton X-100 for 15 min. Cells were then blocked with 1% donkey serum for 30 min, and primary antibodies were used to incubate the cells overnight at 4°C. Finally, the cells were incubated with Alexa Fluor-conjugated secondary antibody for 1 h at room temperature. Every step was followed by two 5-min PBS washes. For nuclear staining, prepared specimens were counterstained with 5 mg/ml DAPI for 5 min and washed with PBS. The specificity of

the antibodies was verified by the knockdown of target proteins. For live-cell imaging, PC-3 cells were transfected with fluorescence protein vectors and cultured in 35-mm glass-bottom dishes (801002, NEST, wuxi, Jiangsu, China). Fluorescence images were obtained from a confocal microscope (Leica, Germany) and analyzed with ImageJ software. For colocalization analyses, approximately 50 cells were counted per experiment.

Cell migration and invasion assays

PC-3 or DU145 cells were seeded at a density of 3×10^4 cells on each side of the culture insert (Ibidi, GmbH, 81176) in complete growth medium. After 24 h, the insert was removed, and the cells were washed twice with PBS. Cells were monitored for up to 48 h in medium containing 1% FBS with or without 10 μM cholesterol, and the images were captured at 0 h to 48 h. Migration was analyzed and quantified using ImageJ.

Invasion assays were performed using transwell plates (8 μm;Corning, Inc.). Briefly, 3.5×10^4 cells inmedium containing 1% FBS with or without 10 μM cholesterol were seeded into the upper compartments of transwell sprecoated with Matrigel (BD). The lower compartments of the chambers contained medium supplemented with 10% FBS. Following 24 h of culture, the cells that traversed the membrane were fixed with 4% formaldehyde, stained using 0.1% crystal violet and imaged with a microscope (IX71-A12FL/PH; Olympus Corporation, Tokyo, Japan). Signal intensity and colocalization were measured with the colocalization plugin of ImageJ software.

Quantitative real-time PCR and RNA-seq

Total RNA from PC-3 cells was prepared using TRIzol. Quantitative PCR was performed in a QuantStudio (TM) 7 Flex System (Life Technologies) as follows: denaturation at 94°C for 5 min, followed by 40 cycles of denaturation at 94°C for 30 s, annealing at 55°C for 30 s, and extension at 72°C for 30 s, with a final extension at 72°C for 10 min.

The PC-3 cell cDNA libraries were prepared according to the manufacturer's instructions (Illumina, USA) and sequenced on a Hiseq2500 platform, and 100-bp paired-end (PE) reads were generated and subjected to quality trimming. High-quality reads were aligned to mm10 in Hisat2. Gene expression was quantified as the number of overlapping reads spanning each gene with HT-seq normalization to the RPKM-determined gene annotation file from Ensembl and the DESeq2 package in R. Differentially expressed genes (DEGs) were also identified by the DESeq2 package (Fold change >1.2 or <0.8). The RNA-seq data were submitted to the Sequence Read Archive (SRA) under Bioproject PRJNA485556 and PRJNA522456.

Animal studies

All protocols involving animals were previously approved by the Ethics Committee for the Use of Experimental Animals of the Suzhou Institute of Biomedical Engineering and Technology, Chinese Academy of Sciences (Suzhou, Jiangsu, China). NOD/SCID/IL-2Rγnull (NSG) mice were purchased from the Jackson Laboratory (Bar Harbor, ME, USA). Daily treatment with 0.5% bile salt/0.5% bile salt & 2% cholesterol commenced 5 days before the shNC, shAPMAP1 (1×10^7) cells were injected into the tail veins of 8-week old male mice. Three weeks later, the mice were sacrificed and livers were fixed in formalin before embedded in paraffin using the routine procedure. Hematoxylin and eosin (H&E) staining was performed on sections from paraffin-embedded livers.

Tissue microarrays and IHC

Tissue arrays were obtained from Alena Biotechnology (PR1921a, Xi'an, Shaanxi, China), and immunohistochemistry was performed as a commercial service. Briefly, the cells were fixed, permeabilized and incubated with 1:50 APMAP antibody (TA054034, OriGene, Beijing, China) or EGFR (GeneTech, Shanghai, clone: EP22)/Vimentin (Maxim, Fuzhou, Fujian, clone: V9) antibodies. Immunostaining was performed with biotinylated secondary antibody, streptavidin peroxidase reagent (Abcam, Cambridge, MA, USA) and metal enhanced DAB colorimetric peroxidase substrate (Maxim, Fuzhou, Fujian, China). Immunostained microarrays were scored by according to the staining intensity (-, +, ++, +++) of each tissue point. All of the patients were enrolled with written informed consent. The study were conducted in accordance with the principles of the Declaration of Helsinki, and

was approved by the Institutional Ethical Review Board of the Suzhou Institute of Biomedical Engineering and Technology, Chinese Academy of Sciences.

Preparation of detergent-free lipid rafts

All procedures were carried out on ice. A total of 2×10^8 cells were washed with PBS, scraped into basal buffer (20 mM Tris-HCl, pH 7.8, 250 mM sucrose, 1 mM CaCl2 and 1 mM MgCl2) and pelleted by centrifugation for 2 min at 250 g. The cells were resuspended in 1 ml of basic buffer, lysed by passage through a needle 20 times and centrifuged at 1,000 g for 10 min. An equal volume of base buffer containing 50% OptiPrep was added to the combined postnuclear supernatants. A 4-ml gradient of 0% to 20% OptiPrep in base buffer was poured on top of the lysate. Gradients were centrifuged for 120 min at 52,000 g in a small ultracentrifuge. Cloudiness was evident through the gradient after centrifugation. Gradients were aliquoted at 0.5 ml per aliquot, and the protein distributions were assessed by Western blotting. Proteome analysis of lipid rafts was performed with ptm-biolab (Hangzhou, Zhejiang, China).

Bioinformatics analysis

The protein-protein interaction network was established with the STRING database (string-db.org). The ontology-based pathway analysis was performed with the Gene Ontology (GO) consortium (gnenontology.org) as described (30). GO terms and Kyoto Encyclopedia of Genes and Genomes (KEGG) pathway were enriched with the clusterProfiler, GOstats, and org.Hs.eg.db package in R as described (31). The bubble plot and chord graph were drawn with ggplot2 and GO plotpackage of R.

Statistical analysis

Data are all presented as the mean ± standard deviation (SD). Comparisons between two groups were performed using two-tailed unpaired Student's t-tests. The associations between staining intensity and clinic pathological patterns were assessed using $\chi 2$ tests. All statistical analyses and graph plotting were performed with GraphPad Prism 5.

Results

Cholesterol induces EMT in PCa cells and this process is dependent on ERK1/2 activation

To explore the potential role of cholesterol in EMT, we treated PCa cells with and without cholesterol. The expression of EMT markers, including E-cadherin, N-cadherin and vimentin were detected by Western blot analysis. The results revealed that the expression levels of N-cadherin and vimentin were increased in 22Rv1, DU145 and PC-3 cells treated with cholesterol compared to the control, while N-cadherin was slightly enhanced in PC-3 cells. Cholesterol inhibited the expression of E-cadherin in all three cell lines (Fig. 1A). Furthermore, cholesterol induced the weak mesenchymal-like morphological features in PC-3 cells (Fig. 1B). We next investigated whether cholesterol had any effects on cell migration and invasion. Correspondingly, wound healing and transwell invasion assays showed that the migration and invasion of PC-3 and DU145 cells were increased by cholesterol treatment (Fig. 1C and 1D, Supplementary Fig. S1A and S1B). However, the addition of simvastatin abrogated the effects of cholesterol on migration, invasion and expression of EMT makers (Supplementary Fig. S1C-S1E). To further explore the potential involvement of signaling pathways in cholesterol-induced EMT, we examined the extracellular regulated protein kinases 1/2 (ERK1/2), protein kinase B (AKT), TGF-β and Wingless/Integrated (WNT) signals, which were summarized regulating EMT(4). Western blot analysis showed increased phosphorylation of ERK1/2 after cholesterol treatment in both PC-3 and DU145 cells (Fig. 1E). To determine whether ERK1/2 signaling affected cholesterol-induced EMT, cells were preincubated with the ERK1/2 inhibitors U0126 and PD098059. Both inhibitors abrogated the phosphorylation of ERK1/2 and restored the expression of EMT markers induced by cholesterol, but PD098059 had the weak effect on the cholesterol-induced vimentin expression in PC-3 cells (Fig.1F). Furthermore, the increased migration and invasion of cells under cholesterol treatment were also reversed after treatment with the two ERK inhibitors (Fig. 1G and 1H, Supplementary Fig. S1F and S1G). These data suggest that the ERK signaling pathway is essential for cholesterol-induced EMT in PCa cells.

Cholesterol promotes the accumulation of EGFR and APMAP in lipid rafts

To dissect the effects of cholesterol at the transcriptional level, we analyzed the RNA

expression profiles of PC-3 cells treated with cholesterol. The transcriptions of 76 protein-coding genes were upregulated, and 167 protein-coding genes were downregulated (Fig. 2A, Supplementary TableS1). We further performed GO enrichment and ontology-based pathway analysis of the DEGs. Pathway analysis revealed that these genes were clustered in the EGFR, WNT and VEGF signaling pathways, which are all involved in EMT (Supplementary Fig. S2A). Interestingly, GO enrichment showed that cholesterol might participate in membrane raft-related processes, such as membrane raft polarization, localization and distribution (Fig. 2B, Supplementary Table S2). These membrane raft-related processes were mostly clustered with MAL, which is specifically able to recruit raft components in plasma membrane (32, 33). The expression of MAL was verified by qPCR (Supplementary Fig. S2B). Additionally, MAL and the other DEGs induced by cholesterol were clustered in other lipid-related processes, including membrane raft organization and myelin sheath (Fig. 2C). These data suggest that cholesterol is involved in many important functions of the lipid raft. Because cholesterol is an important component of the lipid raft, we hypothesized that the effect of cholesterol on EMT was due to the formation of lipid rafts. We performed immunofluorescence staining of PC-3 and 22RV1 cells and found that cholesterol treatment significantly increased the formation of lipid rafts on the cell surface (Fig. 2D). Moreover, MAL knockdown reduced the formation of lipid rafts in cholesterol treated cells (Supplementary Fig.S2C), and also rescued the migration, invasion and EMT maker expression induced by cholesterol treatment (Supplementary Fig. S2D-S2F). To explore which proteins are involved in EMT, tandem mass tag labeling and LC-MS/MS analysis were performed to profile protein expression changes in the lipid rafts of PC-3 cells with and without cholesterol treatment. EGFR, an upstream regulator of ERK1/2, was enriched in the lipid rafts after cholesterol treatment. Furthermore, APMAP, which was recently reported to be associated with the metastasis of colorectal cancer (34), was also increased in the lipid rafts. Western blot analysis of the isolated fractions was performed, and the results showed that EGFR was induced by cholesterol in the lipid rafts, while APMAP was upregulated in both the lipid rafts and non-lipid rafts (Fig. 2E). Moreover, the protein levels of APMAP and EGFR were increased by cholesterol treatment in a dose-dependent manner (Supplementary Fig. S2G and S2H). As cholesterol was able to increase the expression of both APMAP and EGFR, we determined whether APMAP was involved in EGFR accumulation. EGFR-RFP vectors were transfected into APMAP-depleted PC-3 cells and control cells, which were then treated with cholesterol. The fluorescence of EGFR-RFP

was enhanced by cholesterol in control cells; however, the effect of cholesterol on EGFR was almost completely inhibited when APMAP was knocked down (Fig. 2F). At the same time, Western blotting showed that knockdown of APMAP impaired the accumulation of EGFR and consequently reduced the phosphorylation of ERK1/2 induced by cholesterol in PC-3 and 22Rv1 cells (Fig. 2G and Supplementary Fig.S2I). Taken together, these data indicate that APMAP increases the protein level of EGFR induced by cholesterol in PCa cells.

APMAP promotes the EMT of PCa cells through EGFR

Having shown that cholesterol induced the expression of genes involved in the EGFR pathway and lipid rafts, as well as the APMAP-mediated accumulation of EGFR in lipid rafts, we hypothesized that APMAP had effects on EMT in PCa cells. We analyzed the RNA expression profiles of APMAP knockdown PC-3 cells. The transcriptions of 931 protein-coding genes were upregulated, and 943 protein-coding genes were downregulated (Supplementary Fig. S3A, Supplementary Table S3). We further performed GO enrichment and KEGG pathway analysis of the DEGs, which revealed that these genes were clustered in the MAPK, Notch, and adhesion-related signaling pathways as well as steroid biosynthetic and cholesterol metabolic process (Fig 3.A, Supplementary Fig. S3B, S3C, Supplementary Table S4 and Supplementary Table S5). These findings indicate that APMAP and cholesterol may have overlapping function. APMAP knockdown markedly impeded the cholesterol-induced migration of PC-3, DU145 and 22Rv1 cells (Fig. 3B, Supplementary Fig. S3D-G). Similarly, the invasion capability of PC-3 and 22Rv1 cells was reduced by APMAP knockdown (Fig. 3C, Supplementary Fig. S3F-H). The effects of cholesterol on the phosphorylation of ERK1/2 and the expression of E-cadherin and vimentin were significantly blocked in APMAP-depleted PC-3 cells (Fig. 3D). In contrast, the APMAP overexpression promoted migration and invasion, while EGFR inhibitors inhibited this effect (Fig. 3E, 3F, Supplementary Fig. S3I and S3J). Additionally, EGFR inhibitors significantly inhibited ERK activation and abrogated the expression of EMT markers in APMAP-overexpressing cells (Fig. 3G). In addition, *in vivo*, intravenous PC-3 cells from cholesterol-fed group markedly formed more liver metastatic nodules compared to the control group. APMAP knockdown cells reduced the liver metastatic nodules in groups with or without cholesterol fed (Fig.3H and 3I). In consistent with the above findings, metastatic tumors derived from control cells in cholesterol-fed group had consistently higher expression levels

of EGFR ($p<0.05$), APMAP ($p<0.01$) and Vimentin ($p<0.001$) compared to tumors in control group. In cholesterol-fed groups, APMAP knockdown reduced their expression levels (EGFR, $P<0.001$; APMAP, $p<0.05$; Vimentin, $p<0.05$) compare to control cells. (Fig.3J, 3K, Supplementary Fig. S3K and S3L). Taken together, these data demonstrate that APMAP participates in cholesterol-induced EMT by regulating EGFR.

Cholesterol decreases the internalization of EGFR through APMAP

To understand how cholesterol mechanistically promotes the accumulation of EGFR in lipid rafts, we determined whether cholesterol increased the transcriptional expression of EGFR. We first performed quantitative RT-PCR and found that cholesterol had no effect on the mRNA level of EGFR (Fig. 4A), suggesting that APMAP regulation of the EGFR level occurs post translationally. The lysosome inhibitor chloroquine prevented EGFR degradation in control cells, whereas protein levels of EGFR were not further increased by cotreatment with cholesterol (Fig. 4B). We further examined the endogenous EGFR protein level in the presence of cycloheximide, an inhibitor of protein translation. Notably, the stability of EGFR was prominently decreased in APMAP-depleted cells compared to control cells after cholesterol treatment (Fig. 4C). EGFR degradation is well known to depend on internalization (35, 36). Given the evidence that cholesterol inhibits EGFR degradation, we first determined whether this inhibition occurred through internalization of EGFR. Indeed, confocal microscopy showed that the colocalization of EGFR and the early endosomal marker Rab5 was decreased by cholesterol treatment in both cells examined by indirect immunofluorescence (50% vs 38%) (Fig. 4D and Supplementary Fig. S4A) and live cells (23% vs 15%) (Fig. 4E and Supplementary Fig. S4B). Furthermore, the colocalization of APMAP-GFP with Rab5-RFP was increased in the presence of cholesterol (10% vs 42%) (Fig. 4F and Supplementary Fig. S4C). Next, we explored whether APMAP inhibited the internalization of EGFR. Increased colocalization of EGFR with Rab5 was observed in APMAP-depleted PC-3 and 22Rv1 cells relative to control cells with cholesterol treatment (Fig. 4G and Supplementary Fig. S4D-S4F). These data suggest that APMAP regulates the stability of cholesterol-mediated EGFR.

APMAP inhibits EGFR internalization by interacting with EPS15R

To determine how APMAP inhibited the internalization of EGFR, we expressed a 3XFLAG-tagged APMAP or empty vector in PC3 cells. APMAP-3XFLAG was

immunoprecipitated, and expression was confirmed by Western blot (Supplementary Fig.S4G). We used coimmunoprecipitation coupled with label-free comparative LC-MS/MS analysis to identify APMAP-binding partners, revealing hundreds of potential APMAP-binding proteins (Supplementary Table S6). To understand the biological roles of putative targets of APMAP, we performed GO enrichment and pathway analysis using APMAP-binding partners. Pathway analysis revealed that the ubiquitin proteasome, p38 MAPK, Huntington disease, cytoskeletal regulation by Rho GTPase and cell cycle pathways were enriched by these proteins (Supplementary Fig. S4H). Strikingly, three coat protein (COPI) vesicle terms were enriched in the top 20 GO terms (Fig. 5A, Supplementary Table S7). The STRING protein-protein interaction network database revealed the relationships between the top 30 proteins, and these coat proteins formed a COPI complex (Supplementary Fig. S4I). Furthermore, coat proteins and the other proteins that were immunoprecipitated with APMAP were also clustered in other vesicle processes, including retrograde vesicle-mediated transport, Golgi-to-ER vesicular transport and the Golgi-associated vesicle membrane (Fig.5B). These data suggest that APMAP is involved in the infusion of vesicle and vesicle-mediated transport. As EPS15R is involved in EGFR internalization, we first confirmed the physical interaction of endogenous APMAP with EPS15R by co-immunoprecipitation from PC-3 cell lysates (Fig. 5C). We found that the protein level of EPS15R was not affected by cholesterol (Fig. 5D), while plasma membrane immunofluorescence showed that more APMAP colocalized with EPS15R in the membrane when cells were exposed to cholesterol (36% vs 20%) (Fig. 5E and Supplementary Fig. S4J). Consistently, their interaction was enhanced by cholesterol treatment (Fig. 5F). Furthermore, EPS15R increased the interaction with APMAP in cholesterol-treated cells and dissociated with EGFR. (Fig. 5G). Based on these data, we hypothesized that EPS15R was critical for the APMAP-mediated degradation of EGFR. The enhanced recruitment of EGFR to early endosomes by APMAP knockdown was blocked by EPS15R knockdown (37% vs 13% and 14%) in DU-145 cells (Fig. 5H and Supplementary Fig.S4K). Consistently, the protein level of EGFR was restored by EPS15R depletion in APMAP-depleted cells in the presence of cholesterol (Fig. 5I). These results indicate that APMAP inhibits the internalization of EGFR into early endosomes by binding to EPS15R, thus affecting the cholesterol-induced protein stability of EGFR.

APMAP is significantly upregulated in PCa

To understand the role of APMAP in malignancy, we performed bioinformatics analyses of the transcriptional levels of APMAP across 15 types of cancers by comparing tumors with their adjacent normal samples from The Cancer Genome Atlas (TCGA) database. Among 15 types of cancers, the transcriptional APMAP levels between cancer and control samples were similar in breast carcinoma and thyroid carcinoma, significantly lower in cholangiocarcinoma, kidney renal clear cell carcinoma and liver hepatocellular carcinoma and significantly higher in all other 10 cancer types (Fig. 6A). Additionally, APMAP expression was significantly higher in PCa tumors compared with the adjacent normal tissues from both paired and unpaired samples ($P<0.001$) (Fig. 6B). A subsequent receiver operating characteristic (ROC) curve analysis showed the sensitivity and specificity of APMAP expression in predicting PCa tissues from normal tissues. APMAP displayed predictive significance, with an area under the curve (AUC) of 0.752 (Fig. 6C). Gene Expression Omnibus (GEO) datasets showed that the transcriptional level of APMAP was not changed by dihydrotestosterone (DHT) or enzalutamide treated cells (Supplementary Fig. S5A), and in the castration resistance prostate cancer (CRPC) compared with hormone-naïve prostate cancer (Supplementary Fig. S5B-S5E). There is also no significant difference of APMAP expression between CRPC and Neuroendocrine Prostate Cancer (Supplementary Fig. S5F) (37). To evaluate the protein expression of APMAP in PCa tissues compared to normal tissues, immunohistochemical (IHC) staining was performed on tissue microarray samples from 80 PCa patients and 8 normal controls. The results revealed that APMAP protein expression was increased in PCa tissues compared with the normal tissues (Fig. 6D, Supplementary Fig. S6 and Supplementary Table S8). Heterogeneous levels of APMAP were found in 55 out of 80 PCa samples (69%) but only in 2 out of 8 (25%) normal samples. There was also a statistically significant difference between the M1 and M0 tissues (80% vs 67%, $P<0.05$) as well as the N1 and N0 tissues (83% vs 67%, $P<0.05$) (Fig. 6E). Lastly, the results indicated that the expression of APMAP was significantly higher in tumors and suggested APMAP as a potential diagnostic marker for PCa.

DISCUSSION

Cholesterol has been shown to increase the risk of aggressive PCa (13, 38), and consistent with these findings, patients who take statins after prostatectomy have less aggressive PCa (39). Furthermore, cholesterol regulates the proliferation and migration of PCa cells through TRPM7 and the AKT and/or the ERK1/2 pathways (40). Our study

provides further evidence that cholesterol promotes the EMT of PCa cells via the activated ERK1/2 pathway. Cholesterol is an essential component of cell membranes and is enriched in detergent-resistant membrane domains called lipid rafts, where signal transduction actively occurs (41, 42). GO term enrichment showed that membrane raft-related terms were clustered by MAL in cholesterol-treated cells. Cholesterol levels in lipid rafts affect PCa cell viability and apoptosis through the tyrosine phosphorylation of proteins in rafts (22, 43, 44). Increased levels of membrane cholesterol reduce isolated rafts and induce the formation of larger rafts in the cell-free model (45). Consistent with these findings, we proposed that the identification of raft-associated proteins would provide new insight into the signal transduction of cancer progression and the function of cholesterol. Proteome analysis of lipid rafts showed that cholesterol increases APMAP levels in lipid rafts. Our data showed that the cholesterol-mediated upregulation of APMAP stabilized EGFR and subsequently activated ERK1/2 for EMT.

One clinical study showed that APMAP expression may serve as a prognostic biomarker for colorectal cancer with liver metastasis (34). Primary colorectal cancer cells overexpressing APMAP prefer to metastasize to the liver. However, the mechanism underlying this selective metastasis is unclear. All of these findings suggest that APMAP may link obesity to cancer. Emerging evidence has proven that obesity is associated with many cancers, and both diseases can result from an obesogenic diet. Here, we demonstrated that APMAP is upregulated by cholesterol and participates in the progression of EMT and metastasis. Based on these data, one can reasonably believe that APMAP is a key regulator that provides a link between a high-fat diet, obesity and metastasis.

Unbalanced recycling and defective vesicular trafficking of receptors has emerged as a new hallmark of cancers (46). EGFR is endocytosed through clathrin-dependent or lipid raft-dependent pathways. Plasma membrane cholesterol directly controls EGFR activation in laryngeal carcinoma cells (29, 47). The total EGFR level has also been shown to be unaffected by treatment with cholesterol for a short time (30 min), though the EGFR distribution is altered under these conditions, with less EGFR localizing to the plasma membrane . In our study, we found that EGFR expression is increased and accumulated in the lipid rafts of PCa cells treated with cholesterol over a relatively long period of time (48h). Internalization of EGFR depends on interactions with three ubiquitination-related proteins, namely, EPS15, EPS15R, and epsin (29). The independent roles of EPS15 and EPS15R in the

endocytosis of EGFR have been demonstrated by several studies (48, 49).

APMAP knockdown attenuates the cholesterol-induced accumulation of EGFR, implying that the effect of cholesterol on EGFR accumulation is in a partially APMAP dependent manner. In addition, cholesterol enhanced the interaction between APMAP and EPS15R, thereby reducing the internalization of EGFR. EPS15R knockdown rescued the decreased protein level of EGFR in the absence of APMAP. Together, these data demonstrate that EGFR upregulation by cholesterol depends on increased APMAP-EPS15R complex formation. A previous study has shown that APMAP mediates the transport of Aβ from endosomes to lysosomes and subsequently leads to Aβ degradation (50). We also observed that the proteins coimmunoprecipitated with APMAP showed enrichment in vesicle GO terms. These findings suggest that APMAP may regulate the endocytosis of partial membrane proteins in vesicle-dependent transport, in addition to EGFR and Aβ.

Our data provide new insights and an underlying mechanism for the function of APMAP, which enhances binding to EPS15R in the presence of cholesterol, thus increasing EGFR stability to induce the EMT of PCa (Fig. 6F).

Acknowledgments

Funding: This work was supported by the National Key R&D Program of China (2016YFC1302100); National Natural Science Foundation of China (81773023 and 81472827); Hundred-Talent Program and Frontier Research Program (QYZDB-SSW-SMC038) of Chinese Academy of Sciences, to Shan Gao; the Natural Science Foundation of Jiangsu Province (Grant BK20160174) and National Natural Science Foundation of China (81802526) to Siyuan Jiang; the Scientific and Technological Innovation Program of Shanxi Transformation and Comprehensive Reform Demonstration Area of Antibody screening and development platform (2017KJCX01) to Zhou Tong.

Data and materials availability: All data needed to evaluate the conclusions in the paper are present in the paper and/or the Supplementary Materials.

We thank staffs from the Advanced Optical Micro-imaging Platform of Suzhou Institute of Biomedical Engineering and Technology, China Academy of Science for their assistance with imaging experiments.

References and Notes

1. Wu JN, Fish KM, Evans CP, Devere White RW, Dall'Era MA. No improvement noted in overall or cause-specific survival for men presenting with metastatic prostate cancer over a 20-year period. Cancer. 2014;120:818-23.
2. Chambers AF, Groom AC, MacDonald IC. Dissemination and growth of cancer cells in metastatic sites. Nature reviews Cancer. 2002;2:563-72.
3. Zeisberg M, Neilson EG. Biomarkers for epithelial-mesenchymal transitions. The Journal of clinical investigation. 2009;119:1429-37.
4. Iwatsuki M, Mimori K, Yokobori T, Ishi H, Beppu T, Nakamori S, et al. Epithelial-mesenchymal transition in cancer development and its clinical significance. Cancer science. 2010;101:293-9.
5. Chatterjee K, Jana S, DasMahapatra P, Swarnakar S. EGFR-mediated matrix metalloproteinase-7 up-regulation promotes epithelial-mesenchymal transition via ERK1-AP1 axis during ovarian endometriosis progression. FASEB journal : official publication of the Federation of American Societies for Experimental Biology. 2018:fj201701382RR.
6. Lo HW, Hsu SC, Xia W, Cao X, Shih JY, Wei Y, et al. Epidermal growth factor receptor cooperates with signal transducer and activator of transcription 3 to induce epithelial-mesenchymal transition in cancer cells via up-regulation of TWIST gene expression. Cancer research. 2007;67:9066-76.
7. Nakazawa M, Kyprianou N. Epithelial-mesenchymal-transition regulators in prostate cancer: Androgens and beyond. The Journal of Steroid Biochemistry and Molecular Biology. 2017;166:84-90.
8. Montanari M, Rossetti S, Cavaliere C, D'Aniello C, Malzone MG, Vanacore D, et al. Epithelial-mesenchymal transition in prostate cancer: an overview. Oncotarget. 2017;8:35376-89.
9. Mak P, Leav I, Pursell B, Bae D, Yang X, Taglienti CA, et al. ERbeta impedes prostate cancer EMT by destabilizing HIF-1alpha and inhibiting VEGF-mediated snail nuclear localization: implications for Gleason grading. Cancer cell. 2010;17:319-32.
10. Touvier M, Fassier P, His M, Norat T, Chan DS, Blacher J, et al. Cholesterol and breast cancer risk: a systematic review and meta-analysis of prospective studies. The British journal of nutrition. 2015;114:347-57.
11. Freeman MR, Solomon KR. Cholesterol and prostate cancer. Journal of cellular biochemistry. 2004;91:54-69.
12. Wang C, Li P, Xuan J, Zhu C, Liu J, Shan L, et al. Cholesterol Enhances Colorectal Cancer Progression via ROS Elevation and MAPK Signaling Pathway Activation. Cellular physiology and biochemistry : international journal of experimental cellular physiology, biochemistry, and pharmacology. 2017;42:729-42.
13. Pelton K, Freeman MR, Solomon KR. Cholesterol and prostate cancer. Current opinion in pharmacology. 2012;12:751-9.
14. YuPeng L, YuXue Z, PengFei L, Cheng C, YaShuang Z, DaPeng L, et al. Cholesterol Levels in Blood and the Risk of Prostate Cancer: A Meta-analysis of 14 Prospective Studies. Cancer epidemiology, biomarkers & prevention : a publication of the American Association for Cancer Research, cosponsored by the American Society of Preventive Oncology. 2015;24:1086-93.
15. Bravi F, Scotti L, Bosetti C, Talamini R, Negri E, Montella M, et al. Self-reported history of hypercholesterolaemia and gallstones and the risk of prostate cancer. Annals of oncology : official journal of the European Society for Medical Oncology. 2006;17:1014-7.
16. Platz EA, Clinton SK, Giovannucci E. Association between plasma cholesterol and prostate cancer in the PSA era. International journal of cancer. 2008;123:1693-8.

17. Platz EA, Leitzmann MF, Visvanathan K, Rimm EB, Stampfer MJ, Willett WC, et al. Statin drugs and risk of advanced prostate cancer. Journal of the National Cancer Institute. 2006;98:1819-25.
18. Graaf MR, Beiderbeck AB, Egberts AC, Richel DJ, Guchelaar HJ. The risk of cancer in users of statins. Journal of clinical oncology : official journal of the American Society of Clinical Oncology. 2004;22:2388-94.
19. Murtola TJ, Tammela TL, Lahtela J, Auvinen A. Cholesterol-lowering drugs and prostate cancer risk: a population-based case-control study. Cancer epidemiology, biomarkers & prevention : a publication of the American Association for Cancer Research, cosponsored by the American Society of Preventive Oncology. 2007;16:2226-32.
20. Pon D, Abe A, Gupta EK. A review of statin use and prostate cancer. Current atherosclerosis reports. 2015;17:474.
21. Murai T. Cholesterol lowering: role in cancer prevention and treatment. Biological chemistry. 2015;396:1-11.
22. Zhuang L, Kim J, Adam RM, Solomon KR, Freeman MR. Cholesterol targeting alters lipid raft composition and cell survival in prostate cancer cells and xenografts. The Journal of clinical investigation. 2005;115:959-68.
23. Singh G, Sankanagoudar S, Dogra P, Chandra NC. Interlink between cholesterol & cell cycle in prostate carcinoma. The Indian journal of medical research. 2017;146:S38-S44.
24. Pessentheiner AR, Huber K, Pelzmann HJ, Prokesch A, Radner FPW, Wolinski H, et al. APMAP interacts with lysyl oxidase-like proteins, and disruption of Apmap leads to beneficial visceral adipose tissue expansion. FASEB journal : official publication of the Federation of American Societies for Experimental Biology. 2017.
25. Albrektsen T, Richter HE, Clausen JT, Fleckner J. Identification of a novel integral plasma membrane protein induced during adipocyte differentiation. The Biochemical journal. 2001;359:393-402.
26. Bogner-Strauss JG, Prokesch A, Sanchez-Cabo F, Rieder D, Hackl H, Duszka K, et al. Reconstruction of gene association network reveals a transmembrane protein required for adipogenesis and targeted by PPARgamma. Cellular and molecular life sciences : CMLS. 2010;67:4049-64.
27. Ma Y, Gao J, Yin J, Gu L, Liu X, Chen S, et al. Identification of a Novel Function of Adipocyte Plasma Membrane-Associated Protein (APMAP) in Gestational Diabetes Mellitus by Proteomic Analysis of Omental Adipose Tissue. Journal of proteome research. 2016;15:628-37.
28. Carbone R, Fre S, Iannolo G, Belleudi F, Mancini P, Pelicci PG, et al. eps15 and eps15R are essential components of the endocytic pathway. Cancer research. 1997;57:5498-504.
29. Sigismund S, Woelk T, Puri C, Maspero E, Tacchetti C, Transidico P, et al. Clathrin-independent endocytosis of ubiquitinated cargos. Proceedings of the National Academy of Sciences of the United States of America. 2005;102:2760-5.
30. The Gene Ontology C. Expansion of the Gene Ontology knowledgebase and resources. Nucleic acids research. 2017;45:D331-D8.
31. Yu G, Wang LG, Han Y, He QY. clusterProfiler: an R package for comparing biological themes among gene clusters. Omics : a journal of integrative biology. 2012;16:284-7.
32. Ramnarayanan SP, Tuma PL. MAL, but not MAL2, expression promotes the formation of cholesterol-dependent membrane domains that recruit apical proteins. The Biochemical journal. 2011;439:497-504.
33. Magal LG, Yaffe Y, Shepshelovich J, Aranda JF, de Marco Mdel C, Gaus K, et al. Clustering and lateral concentration of raft lipids by the MAL protein. Molecular biology of the cell. 2009;20:3751-62.

34. Mekenkamp LJ, Haan JC, Koopman M, Vink-Borger ME, Israeli D, Teerenstra S, et al. Chromosome 20p11 gains are associated with liver-specific metastasis in patients with colorectal cancer. Gut. 2013;62:94-101.
35. Avraham R, Yarden Y. Feedback regulation of EGFR signalling: decision making by early and delayed loops. Nature reviews Molecular cell biology. 2011;12:104-17.
36. Roxrud I, Raiborg C, Pedersen NM, Stang E, Stenmark H. An endosomally localized isoform of Eps15 interacts with Hrs to mediate degradation of epidermal growth factor receptor. The Journal of cell biology. 2008;180:1205-18.
37. Beltran H, Prandi D, Mosquera JM, Benelli M, Puca L, Cyrta J, et al. Divergent clonal evolution of castration-resistant neuroendocrine prostate cancer. Nature medicine. 2016;22:298-305.
38. Hager MH, Solomon KR, Freeman MR. The role of cholesterol in prostate cancer. Current opinion in clinical nutrition and metabolic care. 2006;9:379-85.
39. Papadopoulos G, Delakas D, Nakopoulou L, Kassimatis T. Statins and prostate cancer: molecular and clinical aspects. European journal of cancer. 2011;47:819-30.
40. Sun Y, Sukumaran P, Varma A, Derry S, Sahmoun AE, Singh BB. Cholesterol-induced activation of TRPM7 regulates cell proliferation, migration, and viability of human prostate cells. Biochimica et biophysica acta. 2014;1843:1839-50.
41. Suzuki KG. [Mechanisms for signal transduction in lipid rafts of cell plasma membranes]. Seikagaku The Journal of Japanese Biochemical Society. 2013;85:34-7.
42. Ohkubo S, Nakahata N. [Role of lipid rafts in trimeric G protein-mediated signal transduction]. Yakugaku zasshi : Journal of the Pharmaceutical Society of Japan. 2007;127:27-40.
43. Oh HY, Lee EJ, Yoon S, Chung BH, Cho KS, Hong SJ. Cholesterol level of lipid raft microdomains regulates apoptotic cell death in prostate cancer cells through EGFR-mediated Akt and ERK signal transduction. The Prostate. 2007;67:1061-9.
44. Oh HY, Leem J, Yoon SJ, Yoon S, Hong SJ. Lipid raft cholesterol and genistein inhibit the cell viability of prostate cancer cells via the partial contribution of EGFR-Akt/p70S6k pathway and down-regulation of androgen receptor. Biochemical and biophysical research communications. 2010;393:319-24.
45. Lawrence JC, Saslowsky DE, Edwardson JM, Henderson RM. Real-time analysis of the effects of cholesterol on lipid raft behavior using atomic force microscopy. Biophysical journal. 2003;84:1827-32.
46. Mosesson Y, Mills GB, Yarden Y. Derailed endocytosis: an emerging feature of cancer. Nature reviews Cancer. 2008;8:835-50.
47. Ringerike T, Blystad FD, Levy FO, Madshus IH, Stang E. Cholesterol is important in control of EGF receptor kinase activity but EGF receptors are not concentrated in caveolae. Journal of cell science. 2002;115:1331-40.
48. Tebar F, Sorkina T, Sorkin A, Ericsson M, Kirchhausen T. Eps15 is a component of clathrin-coated pits and vesicles and is located at the rim of coated pits. The Journal of biological chemistry. 1996;271:28727-30.
49. Huang F, Khvorova A, Marshall W, Sorkin A. Analysis of clathrin-mediated endocytosis of epidermal growth factor receptor by RNA interference. The Journal of biological chemistry. 2004;279:16657-61.
50. Mosser S, Alattia JR, Dimitrov M, Matz A, Pascual J, Schneider BL, et al. The adipocyte differentiation protein APMAP is an endogenous suppressor of Abeta production in the brain. Hum Mol Genet. 2015;24:371-82.

Figures with legends

Fig. 1. Cholesterol induces EMT by ERK1/2 activation in prostate cancer cells. (A) DU145, PC-3 and 22Rv1 cells were treated with 10 μM cholesterol for 48 h and subjected to Western blot analysis using the indicated antibodies. (B) Representative images of the morphology of PC-3 cells treated with 10μM cholesterol for 96 h. Scale bar, 10 μm. (C) Representative images of transwell invasion assays of PC-3 and DU145 cells. (D) Representative images of wound healing assays of PC-3 and DU145 cells. (E) Western blot analysis of PC-3 and DU145 cells treated with 10μM cholesterol for 48 h using the indicated antibodies. (F) PC-3 and 22Rv1 cells were pretreated with or without U0126 (1μM) and PD098059 (20μM) for 1h followed by treatment with cholesterol for 48h. Western blotting was performed to examine the phosphorylation levels of ERK1/2, and the expression levels of EMT-related proteins. (G) Wound healing and transwell invasion (H) assays of PC-3 cells treated with or without U0126 or PD098059 followed by treatment with cholesterol. Data are presented as the means ± SDs from three independent experiments. **P<0.01, ***P<0.001.

Fig. 2. APMAP is involved in the cholesterol-induced EGFR/ERK1/2 pathway. (A) Heatmap of the cluster analysis of the differentially expressed protein-coding genes in PC-3 cells with and without cholesterol treatment (P<0.05). (B) Top 20 enriched GO terms(P<0.01) for protein-coding genes sorted by RichFactor. The color tints indicate the P-values. The size of the circle represents the number of selected genes in the term. RichFactor indicates the percentage of the ratio of genes in the current study vs the total genes in the term. (C) Chord graph representing 21 differentially expressed genes between cholesterol-treated cells and control cells and the association of these genes to the corresponding top 8 raft-related GO terms (P<0.01, sorted by RichFactor). The gene name color code represents the log2 fold change, with blue corresponding to downregulation and red corresponding to upregulation. (D) Representative immunofluorescence images showing the staining of the indicated lipid raft markers in PC-3 and 22Rv1 cells. (E) Detergent-free raft isolation of PC-3 cells was analyzed by Western blot for the indicated protein. (F) Confocal images showing the expression of EGFR-RFP in APMAP-depleted PC-3 cells treated with cholesterol. (G) Western blot analysis of EGFR, APMAP, phosphor-ERK1/2 and total ERK1/2 in APMAP-depleted PC-3 cells treated with cholesterol. Independent experiments were repeated three times. Scale bar,10 μm.

Fig. 3. APMAP regulates EMT in prostate cancer cells. (A) Top 20 enriched GO terms (sort by p-value) for genes in APMAP knockdown PC-3 cells compared to control cells. The color tints indicate the P-values. The size of the circle represents the number of selected genes in the term. RichFactor indicates the percentage of the ratio of genes in the current study vs the total genes in the term. (B) Wound healing assays in APMAP-depleted PC-3 and DU145 cells treated with cholesterol (10μM, 48h). (C) Transwell invasion assays were carried out with APMAP-depleted PC-3 cells that were treated with cholesterol (10μM, 48h). (D) Western blot analysis of the indicated proteins from APMAP-depleted or control cells with or without cholesterol treatment (10μM, 48h). (E) Wound healing assay of APMAP-overexpressing cells treated with the EGFR

inhibitors Erlotinib (1μM) or AZD3759 (1μM). (F) Transwell invasion assay of APMAP-overexpressing DU145 cells treated with EGFR inhibitors. The right panel shows the quantification of invading cells. (G) Western blot showing the indicated proteins in APMAP-overexpressing PC-3 cells treated with Erlotinib or AZD3759. (H) Representative images of liver metastases and H&E staining (100X) of liver at 3 weeks after the injection of $1x10^7$ APMAP knockdown cells or control cells into cholesterol-fed and control mice (n=5 per group). (I) Statistics of metastatic foci by H&E staining counts. (J) Box plot of Vimentin expression in the metastases samples. Comparisons were performed by $\chi 2$ tests. (K) Immunohistochemical staining of EGFR, APMAP and Vimentin expression in liver metastases from four studied groups. Data are presented as the means ± standard deviations from three independent experiments. -: negative, +: low, ++: moderate and +++: high. **P<0.01.

Fig. 4. Cholesterol reduces the internalization of EGFR through APMAP. (A) The mRNA expression of EGFR in cholesterol-treated PC-3 cells. (B) The relative protein expression level of EGFR in DU145 cells treated with cholesterol and/or lysosome inhibitor chloroquine (CQ, 25 μM) for 24 h. (C) Western blot analysis of EGFR and APMAP in control or shAPMAP1-depeleted PC3 cells with cycloheximide (CHX, 10 μg/mL) treatment at the indicated times after a 48h treatment with cholesterol (10 μM). (D) Immunostaining of EGFR and Rab5 in fixed PC-3 cells with or without cholesterol for 48 h. (E and F) PC-3 cells transfected with EGFR-GFP/Rab5-RFP (E) and APMAP-GFP/Rab5-RFP (F) vectors and treated with cholesterol for 48 h. (G) Immunostaining of EGFR (red) and Rab5 (green) in control or APMAP-depleted DU145 cells with or without cholesterol for 48 h. N.S. no significant difference. Scale bar, 10 μm. Arrows indicate colocalization of EGFR and Rab5. Three independent experiments were performed for each analysis.

Fig. 5. APMAP inhibits EGFR internalization by binding to EPS15R. (A) Enrichment of top 20 GO terms (P<0.01) for APMAP-immunoprecipitated proteins in PC-3 cells sorted by RichFactor. The color tints indicate the P-values. The size of the circle represents the number of selected genes in the term. RichFactor expresses the percentage of the ratio of genes in this study vs the total number of genes in the term. (B) The chord graph represents 18 DEGs and the associations of these genes to the corresponding top 10 vesicle-related GO terms;P<0.01 and sorted by RichFactor. The color represents the term. (C) Western blot analysis of the Co-IP assay performed to assess the interaction between APMAP and EPS15R in PC-3 cells. (D) Western blot analysis of cholesterol (10 μM, 48 h)-treated PC-3 cells using the indicated antibodies. (E) Colocalization of EPS15R and APMAP to the plasma membrane of DU-145 cells, without permeabilization. (F) Co-IP assays were performed with anti-APMAP antibodies in the lysates of PC-3 cells treated with cholesterol, followed by immunoblot assays. (G) Co-IP assays were performed with anti-EPS15R antibodies in the lysates of PC-3 cells treated with cholesterol, followed by western blot assays. (H) Immunostaining of EGFR and Rab5 in cholesterol-treated DU145 cells with shAPMAP1 depletion and/or knockdown of EPS15R by siRNA. (I) Western blot showing the protein levels of EGFR, EPS15, and APMAP in cells with shAPMAP depletion

and/or concurrent knockdown of EPS15R in PC-3 cells. Scale bar, 10 μm. Arrows indicate the colocalization of EGFR and Rab5. Three independent experiments were performed for each analysis.

Fig. 6. APMAP is upregulated in PCa. (A) The boxplot shows the expression levels of APMAP in adjacent normal and tumor tissues across 15 TCGA cancer types. (B) APMAP mRNA expression in paired and unpaired TCGA PCa samples. (C) ROC curves of APMAP for predicting the clinical diagnostic value of APMAP in PCa based on the TCGA database. (D) Immunohistochemical staining of prostate and normal tissues for APMAP expression. (E) Box plot of APMAP expression in the PCa samples. The subjects were divided into four groups based on their APMAP expression scores, representing negative, low, moderate and high expression. Data were analyzed with the rank-sum test. (F)The proposed model for cholesterol-induced EMT via accumulation of APMAP in lipid rafts, preventing internalization of EGFR and thus inducing the EGFR/ERK1/2 signaling pathway, is shown. Under conditions of added cholesterol, cytosolic EPS15R is bound to APMAP, which stabilizes EGFR on lipid rafts to inhibit its internalization. -: negative, +: low, ++: moderate and +++: high. *, $P<0.05$, **, $P<0.01$, ***, $P<0.001$; M1, patients with metastasis, M0, patients without metastasis; N1, patients with lymph node involvement, N0, patients without nodal involvement.

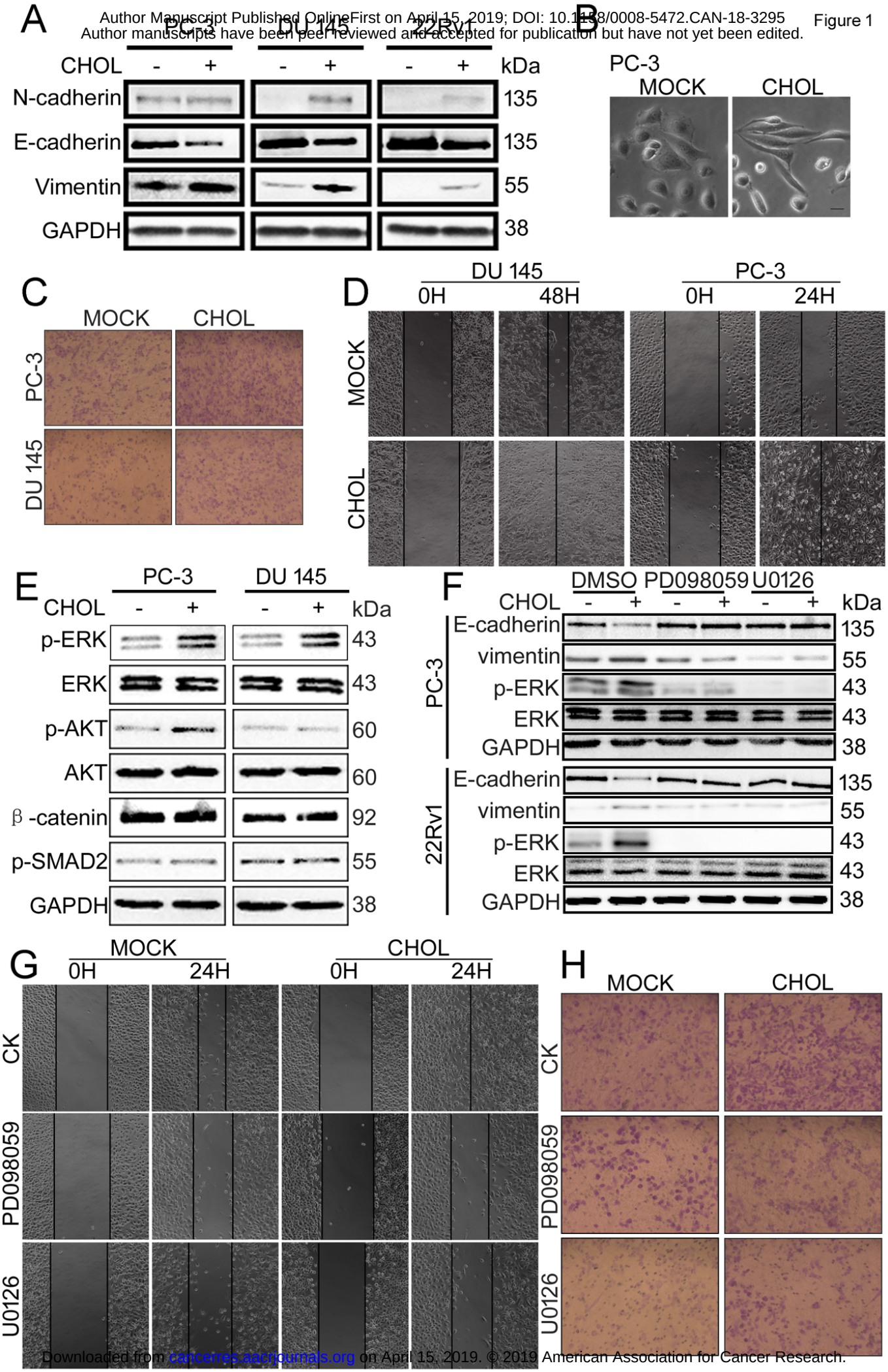

Author Manuscript Published OnlineFirst on April 15, 2019; DOI: 10.1158/0008-5472.CAN-18-3295
Author manuscripts have been peer reviewed and accepted for publication but have not yet been edited.

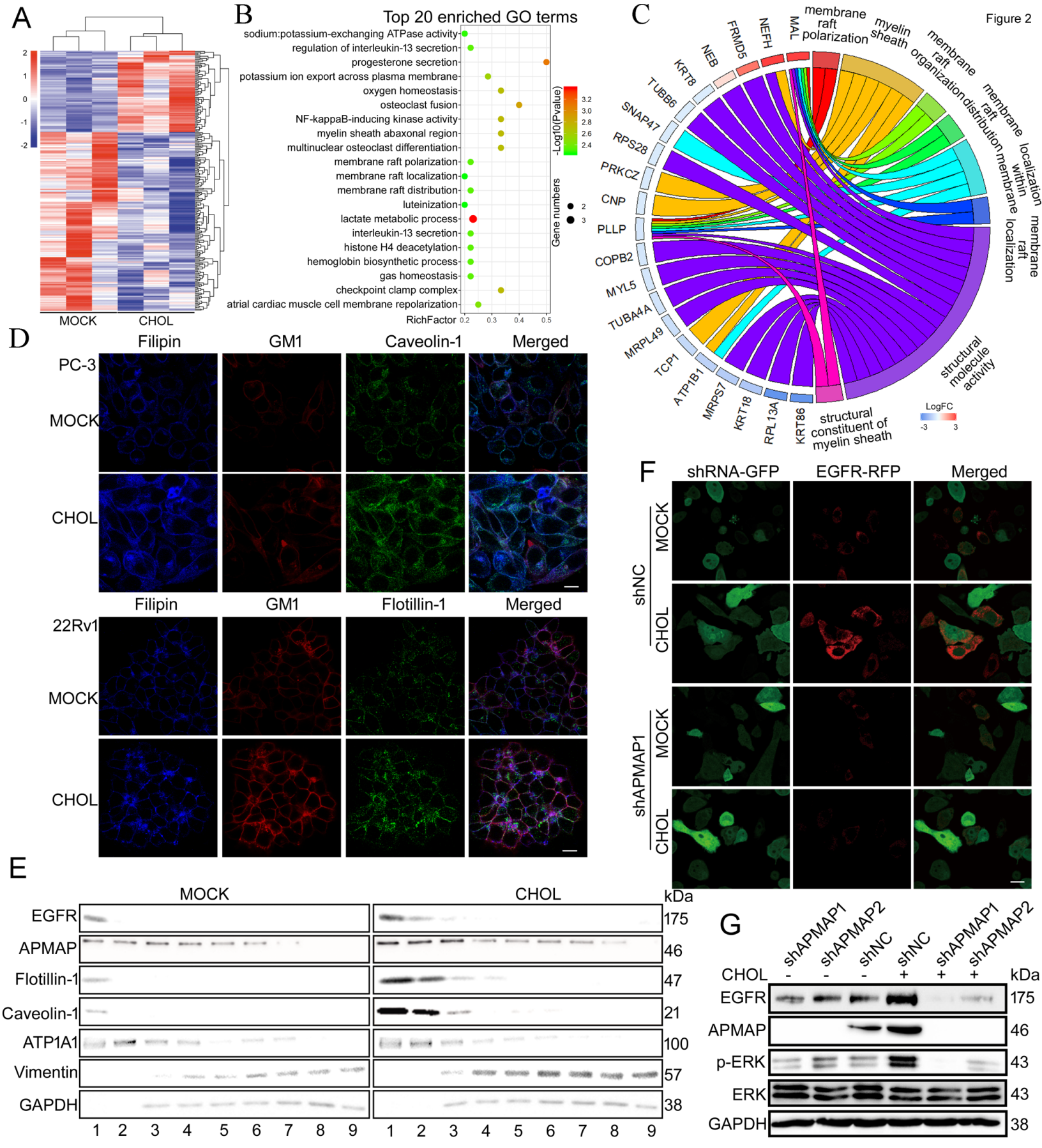

Author Manuscript Published OnlineFirst on April 15, 2019; DOI: 10.1158/0008-5472.CAN-18-3295
Author manuscripts have been peer reviewed and accepted for publication but have not yet been edited.

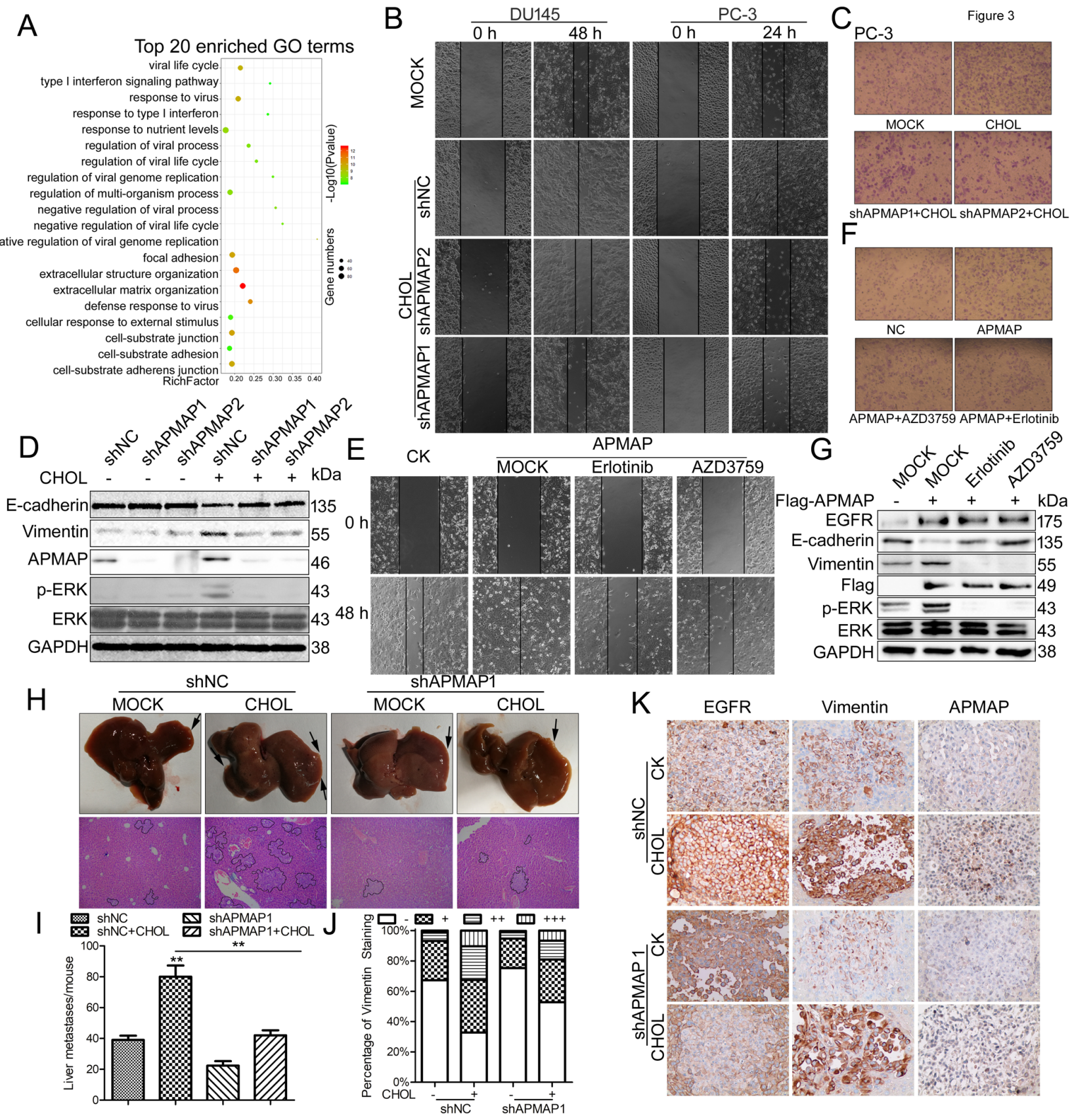

Author Manuscript Published OnlineFirst on April 15, 2019; DOI: 10.1158/0008-5472.CAN-18-3295
Author manuscripts have been peer reviewed and accepted for publication but have not yet been edited.

Figure 4

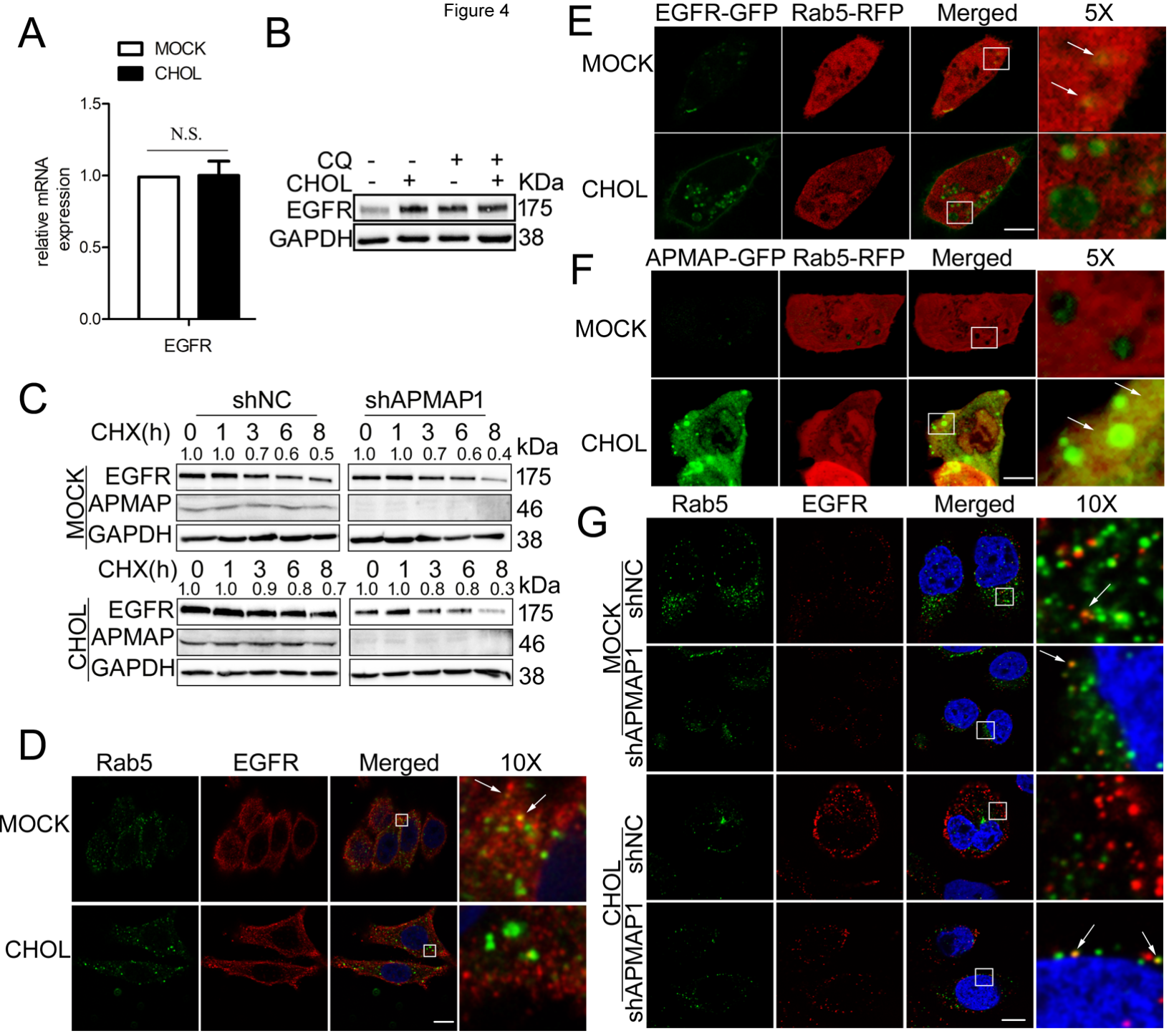

Author Manuscript Published OnlineFirst on April 15, 2019; DOI: 10.1158/0008-5472.CAN-18-3295
Author manuscripts have been peer reviewed and accepted for publication but have not yet been edited.

Figure 5

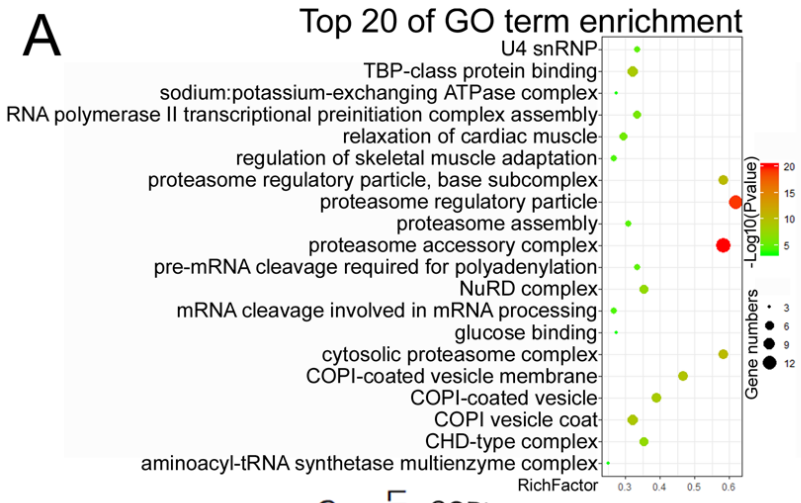

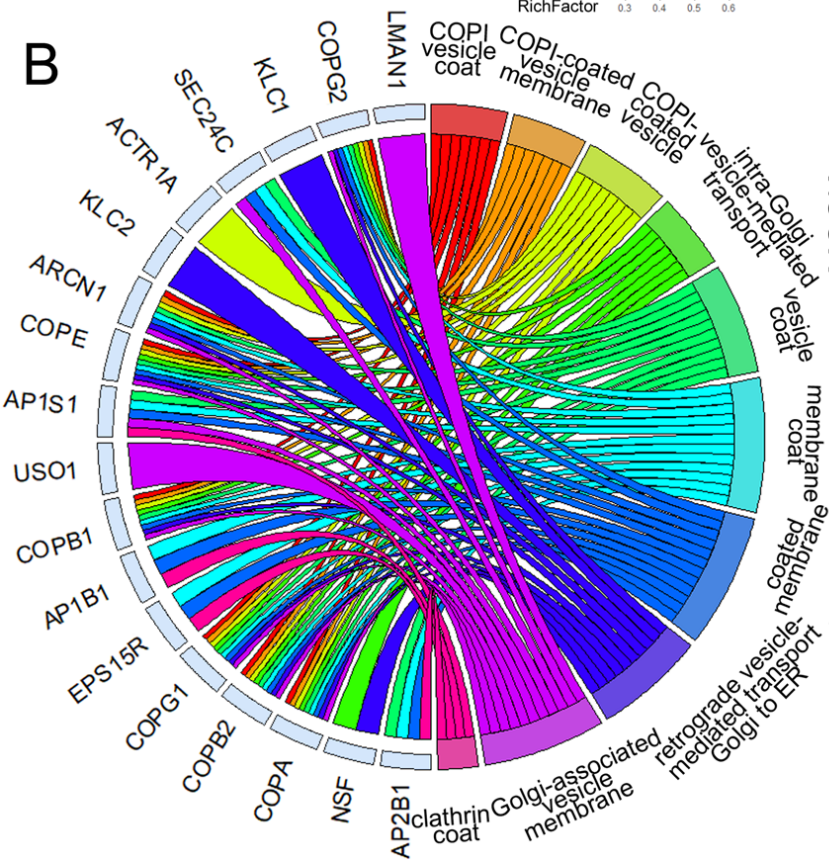

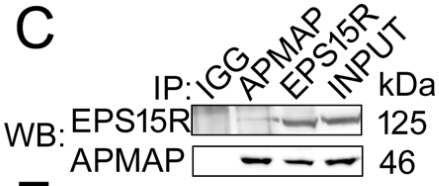

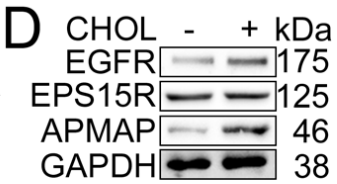

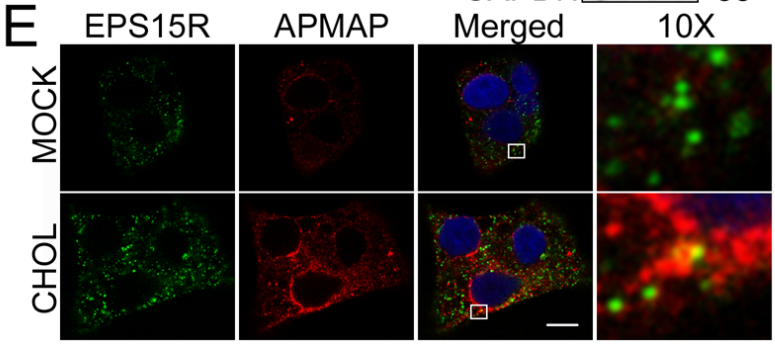

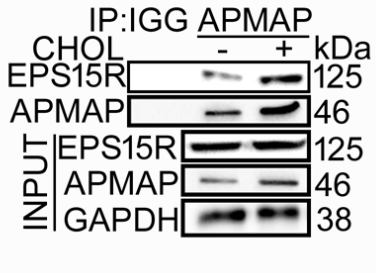

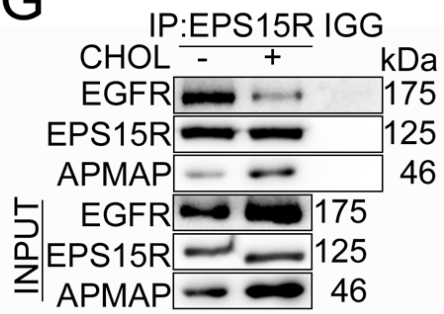

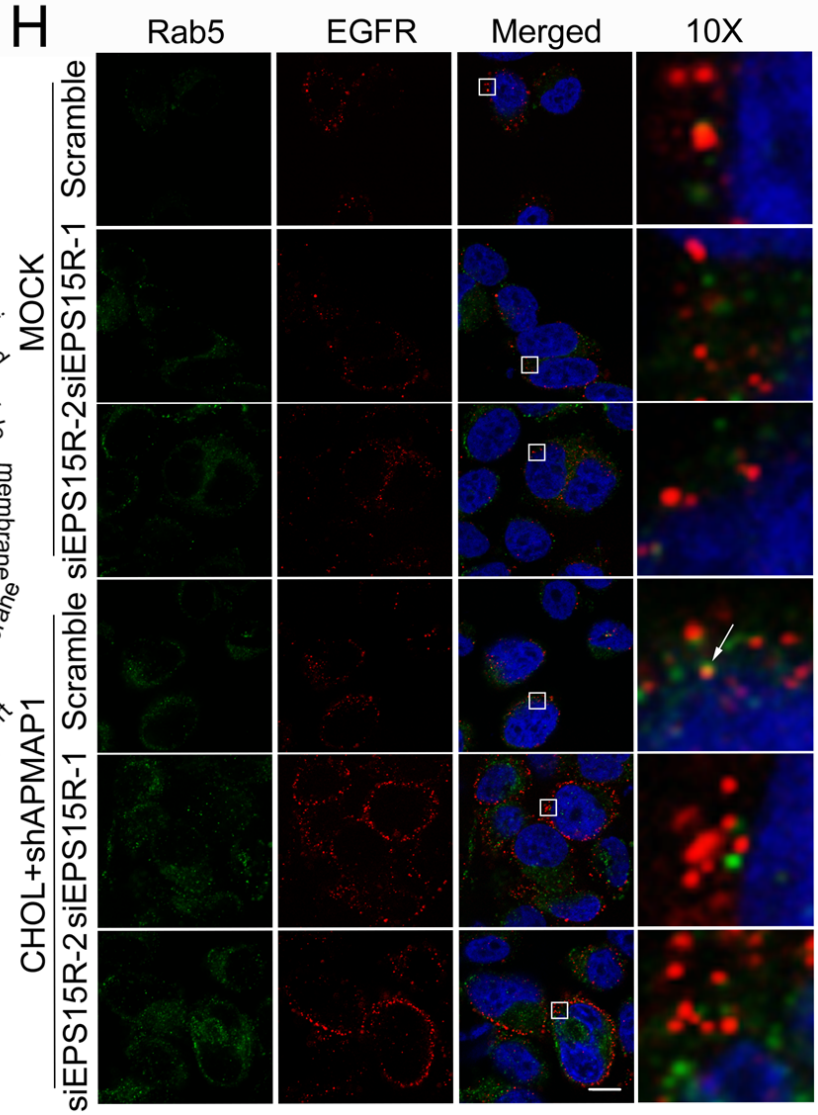

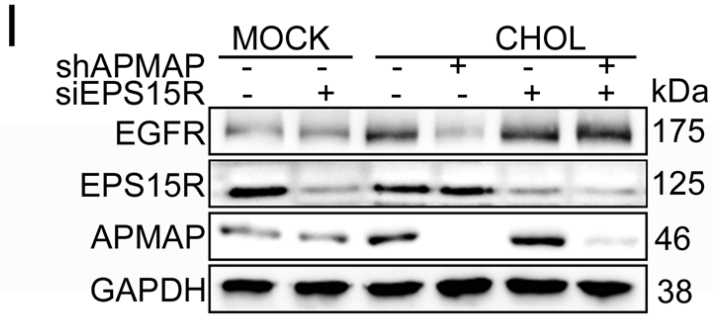

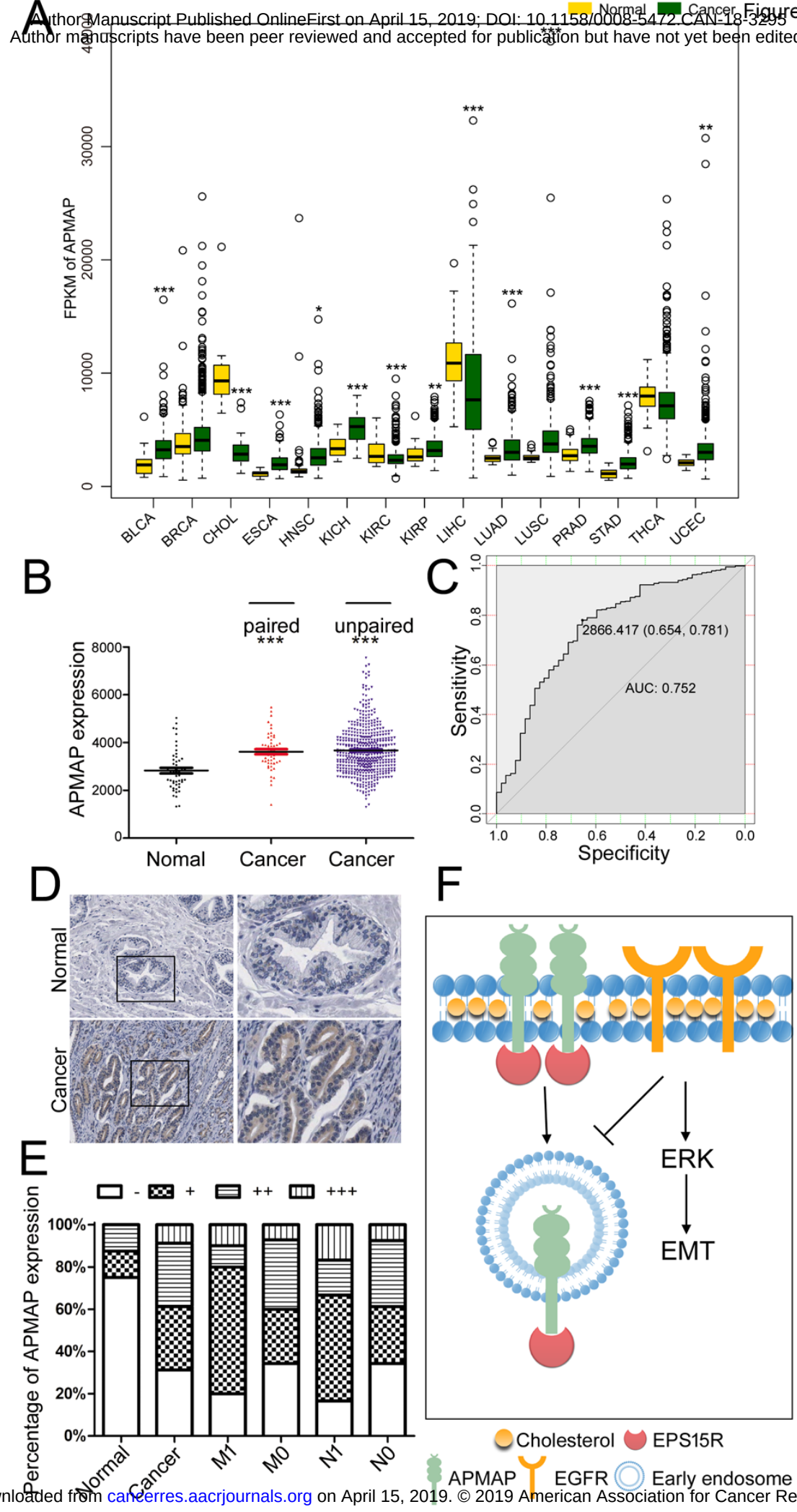

Cancer Research
The Journal of Cancer Research (1916–1930) | The American Journal of Cancer (1931–1940)

AACR American Association for Cancer Research

Cholesterol induces epithelial-to-mesenchymal transition of prostate cancer cells by suppressing degradation of EGFR through APMAP

Siyuan jiang, Xuetong wang, Dalong song, et al.

Cancer Res Published OnlineFirst April 15, 2019.